Raman spectroscopy studies of apatite-type germanate oxide ion conductors: correlation with interstitial oxide ion location and conduction

A. Orera[1*], M.L. Sanjuán[2], E. Kendrick [3], V.M. Orera[2], P.R. Slater[1]

[1] School of Chemistry, University of Birmingham, Birmingham B15 2TT. UK

[2] Instituto de Ciencia de Materiales de Aragón, C.S.I.C.-Universidad de Zaragoza, E-50.009 Zaragoza, Spain

[3] Chemical Sciences, University of Surrey, Guildford, Surrey. GU2 7XH, UK.

[*]Correspondence to:

Dr. A. Orera

School of Chemistry, University of Birmingham, Birmingham B15 2TT. UK

Tel. +44 (0)121 4148906

Fax +44 (0)121 4144403

a.orera@bham.ac.uk

Abstract

A Raman spectroscopy study of the apatite series $La_{8+x}Ba_{2-x}(GeO_4)_6O_{2+x/2}$ is presented. The results show the presence of a new Raman band appearing at ~ 645 cm^{-1}, whose intensity increases with increasing interstitial oxide ion content. This new band is also observed in samples containing cation vacancies, consistent with previous suggestions that the presence of cation vacancies enhances Frenkel defect formation. The fact that the new band is in the stretching region of the spectra, rather than the bending region as observed for the silicate analogues, is consistent with the interstitial oxide ions being more closely associated with the Ge. This band is attributed to the presence of interstitial oxide ions leading to the formation of five coordinate Ge, in agreement with recent neutron diffraction and modelling studies. From the observation of a reduction in the intensity of this band with increasing temperature, it is suggested that the activation energy for conduction in these apatite germanates is a combination of the energy to "free" the interstitial oxide ions from the five coordinate Ge, and the energy for their subsequent migration. The former process is ascribed to the observed reduction in Raman intensity with an activation energy of 0.32 ± 0.06 eV. Thus the higher activation energy for the germanate apatites over the related silicates can be ascribed to the defect trapping associated with the closer association of the interstitial oxide ion with the tetrahedra in the former.

Keywords: Apatite, Raman spectroscopy, oxide ion conductor, defect trapping

Introduction

Materials showing high oxide ion conductivity have attracted considerable interest for applications such as electrolytes in solid oxide fuel cells, oxygen sensors and separation membranes. In most systems, e.g. in fluorite and perovskite structures, oxide ion conduction proceeds via oxide ion vacancies incorporated through suitable cation doping. In contrast, the key defects in the recently reported [1-4] apatite-type silicates/germanates, $Ln_{9.33+x}(Si/GeO_4)_6O_{2+3x/2}$ (Ln=rare earth) (figure 1), are interstitial oxide ions [5-14]. These systems show high conductivities (>1 x 10^{-2} Scm^{-1} at 800°C) when suitably doped, and this has led to a large body of literature aimed at understanding the factors that influence their conductivities [1-33]. A particular focus of our work has been to gain a qualified understanding of the accommodation of the interstitial oxide ions within the structure and their migration mechanism. Computer modelling work has indicated that the most favourable interstitial sites are adjacent the Si/GeO_4 tetrahedra [8,12,13], which has subsequently been supported by experimental work [5-7,9-11,14]. The modelling work also indicated that the migration of these interstitial oxide ion defects was via a complex mechanism involving considerable relaxation of the Si/GeO_4 network. Considering the location of the interstitial oxide ions adjacent to the Si/GeO_4 tetrahedra, and their proposed importance in aiding the conduction process, further information on the local environment around these tetrahedra is warranted. In this respect we recently reported a combined ^{29}Si NMR and Raman spectroscopy study of the series $La_{8+x}Sr_{2-x}(SiO_4)_6O_{2+x/2}$, which showed that the presence of interstitial oxide ions influenced both spectra [15]. For the ^{29}Si NMR

spectra, a second peak attributed to a SiO_4 tetrahedra adjacent to an interstitial site was observed, while in the Raman spectra, a new mode at 360 cm^{-1} appeared for samples with $x>0$ in the symmetric bending mode energy region of the SiO_4 group. The intensities of both the second ^{29}Si NMR peak and new bending mode were shown to increase with increasing oxygen (and hence interstitial) content. This work, hence, showed the complementary features of ^{29}Si NMR and Raman studies in assessing the influence of interstitial oxide ions on the SiO_4 substructure, with the prospect of using both methods to gain an insight into the interstitial defect model and to potentially screen these materials for interstitial oxide-ion content and hence probable oxide-ion conductivity.

In this paper, we extend this study to investigate in detail the Raman spectra of a range of germanate apatites, $La_{8+x}Ba_{2-x}(GeO_4)_6O_{2+x/2}$, to examine whether similar features are observed.

Experimental

The apatite series $La_{8+x}Ba_{2-x}(GeO_4)_6O_{2+x/2}$ (x = 0, 0.4, 0.8, 1.2) with x/2 oxygen interstitials per unit formula were prepared, as described previously [19], by solid state reaction from dried La_2O_3, $BaCO_3$ and GeO_2 starting materials, using two consecutive 10h firing stages at 1100°C with intermediate regrind and a final heating at 1300-1400°C for 2 hours. In order to study the effect of cation vacancies, two other samples were prepared similarly with the compositions $La_{8.6}Ba_{1.2}(GeO_4)_6O_{2.1}$ and $La_{8.83}Ba_{0.75}(GeO_4)_6O_2$. These two compositions were chosen because of their high conductivities (Table 1 [19]). Phase purity was confirmed by X-ray powder diffraction (Panalytical X'Pert Pro diffractometer, Cu $K\alpha_1$ radiation).

Raman dispersion measurements were performed in backscattering geometry, using an optical microprobe spectrometer (Model XY, Dilor, France) with a CCD detector. Spectra were taken at RT with a X10 microscope objective lens in a 10 microns diameter sample region. The power of the laser line was 40mW and the spectral resolution 1.4 cm^{-1}. Spectra at temperatures between 300 and 1073K were measured by putting the sample in a LINKAM TS1500 stage with a temperature stability of 0.5K, and using a X50 long working distance objective lens. In this case the measured area was about 4μm^2. The 514.5 nm line of an Ar^+-ion laser (Model INNOVA 305, Coherent, Palo Alto, CA) was used for sample excitation and the Si Raman line at 520 cm^{-1} for wavelength calibration.

In order to provide more information about the nature of the Raman bands, atomistic potential modelling of two systems, one stoichiometric ($La_8Ba_2(GeO_4)_6O_2$), and one containing oxygen excess ($La_9Ba(GeO_4)_6O_{2.5}$), were performed. The simulations were performed using the GULP code [34, 35], and a detailed description of these atomistic potential methods can be found elsewhere [36, 37]. In brief, the method describes the potential energy of the crystal lattice in terms of long range coulombic terms and short range repulsion and dispersive forces, as described by the Buckingham potential (Eq 1).

$$V_{ij} = A_j \exp\left(\frac{-r}{\rho_{ij}}\right) - \frac{C_{ij}}{r^6} \qquad (1)$$

In order to describe the polarisability of the oxygen atom a shell model is employed, where the shell representing the valence electrons is connected to the core via a harmonic spring constant k. The polarisability of the free ion can therefore be described as:

$$\alpha = Y^2/k \qquad (2)$$

where Y is the charge.

A summary of the interatomic potentials used are given in the supplementary data. With these interatomic potentials, energy minimisation techniques are employed to determine the lowest energy configuration with respect to the atomic positions. Using the energy minimised atomic positions, the properties of the systems can be calculated in more detail. In this work phonon calculations were performed for correlation with the experimental Raman spectra, similar to those described previously by Ammundsen *et al.* for lithium manganese oxides [38]. The calculated eigen states were projected onto the atomic positions, and in this way the atoms and bonds associated with each frequency could be determined.

Results and discussion

Figure 2 shows the Raman spectra for $La_{8+x}Ba_{2-x}(GeO_4)_6O_{2+x/2}$ (x= 0 and 1.2) measured at 300K. From previous studies [24], the bands observed from 700 to 800 cm^{-1} can be assigned to the symmetric ν_1 and asymmetric ν_3 stretching modes and those in the 400 to 500 cm^{-1} region to the ν_4 bending internal modes of the GeO_4 tetrahedra. The strong band at 342 cm^{-1} corresponds to the ν_2 symmetric bending mode and those at lower energies mainly to the translational and librational external modes of the GeO_4 group. The vibration of the channel oxygen is not identified but is expected to appear in the 300-500 cm^{-1} region. An additional mode at 645cm^{-1}, whose intensity increases with increasing interstitial anion content, is observed in the stretching mode region for the samples with x>0. It is important to note that, in contrast to what was observed in the silicate systems [15], this “extra” mode appears in the stretching rather than in the bending region. Note that this mode was also

observed by Rodriguez-Reyna et al [24] in $La_{9.56}(GeO_4)_6O_{2.34}$, although no assignment was made.

In order to accurately study the dependence of the intensity of the mode at 645cm^{-1} with the interstitial oxygen content, and due to the strong lattice disorder broadening of the spectral lines in these germanates, we have performed a lineshape analysis of the spectra in the region from 600 to 850 cm^{-1}, which contains the extra band (I) and the ν_1 and ν_3 internal modes of the GeO_4 tetrahedron. The bands were decomposed using Pseudo-Voigt profiles. This lineshape analysis indicated a linear variation of the intensity of the additional 645 cm^{-1} band, normalised to that of the sum of the high energy group (ν_1 and ν_3 modes), as a function of the interstitial anion content (Fig. 3). Similarly figure 4 shows an increase in conductivity with the increase in the intensity of this band, consistent with the importance of interstitial oxide ions for the conduction process in these apatite systems.

Regarding the samples with non stoichiometric cation content, $(La,Ba)_{10-y}(GeO_4)_6O_{2+x}$ with *y* cation vacancies and *x* "hyperstoichiometric" oxygen interstitials per unit formula, conductivity measurements (Table 1, [19]) showed an enhancement in conductivity for $La_{8.6}Ba_{1.2}(GeO_4)_6O_{2.1}$ and $La_{8.83}Ba_{0.75}(GeO_4)_6O_2$. This enhancement has been attributed to an increase of the interstitial oxygen levels through enhanced Frenkel defect formation, as proposed previously for related silicate apatites containing cation vacancies [4,5,15,25]. In both these samples, the 645 cm^{-1} band is also present, as shown in figure 5, indicating that the effect on the GeO_4 tetrahedra is similar and thus the nature of the interstitial site, whether originating from oxygen hyperstoichiometry or Frenkel defect formation, is closely related. Assuming that the intensity of this band is roughly proportional to the amount of interstitial oxygen and comparing with the samples without cation vacancies, we

can estimate the total amount of interstitial oxygen per formula unit as 0.2 for these samples. This value would imply that approximately one Frenkel-type interstitial is created for every two cation vacancies present in the $La_{8.6}Ba_{1.2}(GeO_4)_6O_{2.1}$ and $La_{8.83}Ba_{0.75}(GeO_4)_6O_2$ samples. Comparing the conductivities of these materials with those observed for the samples without cation vacancies and similar interstitial oxygen content (0.2), there seems to be an enhancement in conductivity for low oxygen excess levels when cation vacancies are introduced. The origin of this is presently unclear and warrants further study, although it has been suggested that the presence of cation vacancies may open up additional conduction pathways in the a,b directions due to the significant distortion around these vacancies [26].

The fact that the new band is in the stretching region of the spectra, rather than the bending region as observed for the silicates, is consistent with the interstitial oxide ions being more closely associated with the Ge. This is in agreement with modelling and neutron diffraction work, which has suggested that the presence of interstitial oxide ions leads to the formation of five coordinate Ge [11,12,14,33].

In order to gain more information about the nature of the additional Raman band, modelling studies were performed. Static lattice energy minimisation was performed for the two materials $La_8Ba_2(GeO_4)_6O_2$ and $La_9Ba(GeO_4)_6O_{2.5}$, with the same interatomic potentials being used in both calculations. Initial calculations were performed using the P63/m symmetry space group, however, significant strain was observed in the lattice for the oxygen excess system due to the very low level of partial occupancy of the interstitial site. Therefore the symmetry constraints were removed, and the calculations performed with space group P1. The interstitial oxygen was located in a position between two GeO_4

units (0.034 0.49 -0.0281), in agreement with prior neutron diffraction and modeling studies [11,12,14,33]. In order to determine the validity of the simulations, the calculated cell parameters were compared with the experimentally observed values, showing good agreement (see supplementary data). It should be noted that with excess oxygen, the lower symmetry P1 space group employed results in a slight triclinic distortion, although from laboratory X-ray diffraction studies the structure appears hexagonal. In this respect, however, it should be noted that such subtle distortions are difficult to observe within the resolution of conventional laboratory X-ray diffraction, appearing simply as a slight broadening of some peaks. Moreover, since the occupancy of interstitial sites is random, the average, long-range structure may appear as hexagonal in X-ray diffraction, despite the presence of local distortions. Indeed, recent studies of related Sr doped apatite germanates using high resolution synchrotron X-ray data have shown subtle distortions, not resolvable by laboratory X-ray data [39], and demonstrated that in this case, the comparable composition $La_9Sr(GeO_4)_6O_{2.5}$ is indeed triclinic.

The phonon and eigenvalue calculations were performed using the energy minimised crystal lattice system, and the IR and Raman active frequencies were calculated. All 33 Raman active modes corresponding to $La_8Ba_2Ge_6O_{26}$ were identified from the displacements of the atoms (see supplementary information, were they are roughly compared to the experimental values). There is a clear shift in frequencies that comes up from the ab-initio character of the calculations, since the potential parameters have not been adjusted to fit the experimental Raman data. However, the main purpose of these calculations has been the investigation of the extra mode related to the presence of interstitial oxygen, and this is possible from the comparison of the results obtained for

$La_8Ba_2(GeO_4)_6O_2$ and $La_9Ba(GeO_4)_6O_{2.5}$. The modelling of the oxygen-hyperstoichiometric system predicts an extra mode in the gap region at ν~675 cm^{-1}, not far from the experimental value of the extra band (645 cm^{-1}). Besides, the eigenvector of the additional mode shows that it is associated with the stretching of the Ge-O bonds of the GeO_5 unit formed with the interstitial oxygen (Figure 6), consistent with an increase in intensity of this mode with increasing interstitial oxygen (and hence GeO_5) concentration.

In order to get additional information on the dynamics of these materials from spectroscopic studies, we have performed high temperature Raman measurements of two compositions of the series: x=1.2 (high interstitial oxygen content) and x=0 (no oxygen interstitials). Figure 7 shows both series of spectra, with *T* varying from RT to 800 ºC.

Spectra have been divided by the prefactor (n(ω,T)+1) affecting the Raman intensities, where n(ω,T) is the Bose-Einstein factor, n(ω,T)=1/(exp(ħω/kT)-1).

Except for a general band broadening and slight softening, the spectra of both samples preserve the basic features as *T* is raised, which implies that no dramatic structural change occurs in this temperature range. However, for the x=1.2 sample there is a decrease in the intensity of the extra (645 cm^{-1}) band with increasing temperature. Consequently, the spectra at 800 ºC look very similar in both compounds, despite the differences in the concentration of cations and interstitial oxide ions and mobility properties. The spectra of the samples after heating, are identical to those obtained at RT before heating, implying that any change undergone by the samples is reversible. In particular, this also means that the mobile oxide ions return to the same sites initially occupied.

As concerns the oxygen dynamics, the most interesting observation is the disappearance of the band at 645 cm^{-1} on increasing *T* in Fig 7(a). In Fig 8 we present a plot of the relative integrated intensities, $I_r = I_I/(I_{v1} + I_{v3})$, as a function of temperature. The continuous line shows the fitting of the data to an expression of type $I_r = I_r^0 - A\exp(-E_a^R/kT)$ with parameters $I_r^0 = 0.042$, $A = 1.3 \pm 0.5$ and $E_a^R = 0.32 \pm 0.06$ eV.

The thermally activated decrease of the band above ~300 ºC can be unambiguously ascribed to the onset of significant oxide ion conduction in this material. However, the activation energy deduced from the band intensity decay is much smaller than that found from conductivity measurements ($E_a^\sigma \sim 1$ eV (table 1)), which suggests that each technique is probing a different process.

According to the calculations presented, the band at 645 cm^{-1} can be attributed to the vibration of five coordinate Ge entities that are created by the incorporation of interstitial oxygen. Assuming that the diffusion mechanism consists of thermally activated jumps of interstitial oxide ions between equivalent sites, we would expect the Raman signal of the extra band to be observed as long as the residence time in each site is long enough to allow the nearby tetrahedra to relax to their equilibrium configurations. On increasing temperature this process may not be fast enough, in the time scale of oxygen mobility, thus explaining the disappearance of the extra band.

Within this model, the activation energy derived from Raman intensities is most likely related to the trapping energy associated with the formation of five coordinate Ge units. As the temperature is increased the interstitial oxide ions become “free” from the Ge units, and hence the intensity of the band at 645 cm^{-1} decreases. Thus the activation energy for conduction (≈1 eV) is a combination of the trapping energy (0.3 eV) and the

energy for their subsequent migration (1-0.3= 0.7 eV). Interestingly this latter value is similar to that observed for silicate apatites, where there is less association of the interstitial oxide ions with the SiO_4 tetrahedra [4,8,9,15]. Moreover, this is consistent with our prior molecular dynamics modeling studies of the related $La_{9.33}(GeO_4)_6O_2$ system, for which the activation energy was calculated to decrease from 0.98 eV to 0.61 eV at high temperatures [12].

Conclusions

We have established a correlation between the concentration of interstitial oxide ions in $La_{8+x}Ba_{2-x}(GeO_4)_6O_{2+x/2}$ and the intensity of a new Raman band appearing at $\nu\sim 645\ cm^{-1}$. This band is attributed to the presence of interstitial oxide ions resulting in the formation of five coordinate Ge, which is consistent with recent neutron diffraction studies and modeling predictions. In the case of compounds with cation deficiency, this extra band is also observed, attributed to the production of oxygen Frenkel-type interstitials (one produced for every two cation vacancies). High temperature Raman studies show that the intensity of this band decreases with increasing temperature, which is attributed to the excitation of the interstitial oxide ion creating a "free" interstitial. The activation energy for this process is found to be 0.32 ± 0.06 eV. Thus the higher activation energy for the apatite germanates compared to the silicates is most likely related to the close association of the interstitial oxide ions with the tetrahedra for the former, resulting in an additional defect trapping energy contribution to the oxide ion conduction activation energy.

Acknowledgements

We would like to thank EPSRC for funding (grant EP/F015178/1) and financial support from the Spanish Ministry of Science and Innovation through project MAT2007-64486-C07-02.

References

1. S. Nakayama, H. Aono, Y. Sadaoka, Chem. Lett. (1995) 431.

2. S. Nakayama, M. Sakamoto, M. Higuchi, K. Kodaira; J. Mater. Sci. Lett. 19 (2000) 91.

3. H. Arikawa, H. Nishiguchi, T. Ishihara, Y. Takita, Solid State Ionics 136-137 (2000) 31.

4. E. Kendrick, M.S. Islam, P.R. Slater; J. Mater. Chem. 17 (2007) 3104.

5. J.E.H. Sansom, D. Richings, P.R. Slater, Solid State Ionics 139 (2001) 205.

6. L. Leon-Reina, M.C. Martin-Sedeno, E.R. Losilla, A. Cabeza, M. Martinez-Lara, S. Bruque, F.M.B. Marques, D.V. Sheptyakov, M.A.G. Aranda; Chem. Mater. 15 (2003) 2099.

7. L. Leon-Reina, E.R. Losilla, M. Martinez-Lara, S. Bruque, M.A.G. Aranda; J. Mater. Chem. 14 (2004) 1142.

8. J.R. Tolchard, M.S. Islam, P.R. Slater; J. Mater. Chem. 13 (2003) 1956.

9. J.E.H. Sansom, J.R. Tolchard, D. Apperley, M.S. Islam, P.R. Slater; J. Mater. Chem. 16 (2006) 1410.

10. L. Leon-Reina, J.M. Porras-Vasquez, E.R. Losilla, M.A.G. Aranda; J. Solid State Chem. 180 (2007) 1250.

11. S. S. Pramana, W.T. Klooster and T. J. White; Acta Cryst. B 63 (2007) 597.

12. E. Kendrick, M.S.Islam, P.R. Slater; Chem. Commun (2008) 715.

13. A. Jones, P.R. Slater, M.S. Islam; Chem Mater 20 (2008) 5055.

14. S.S. Pramana, W.T. Klooster, T.J. White; J. Solid State Chem. 181 (2008) 1717.

15. A. Orera, E. Kendrick, D. C. Apperley, V.M. Orera, P.R. Slater; Dalton Trans. (2008) 5296.

16. J.E.H. Sansom, P.R. Slater; Solid State Ionics 167 (2004) 23.

17. H. Yoshioka; J. Amer. Ceram. Soc. 90 (2007) 3099.

18. E. Kendrick, P.R. Slater; Mater. Res. Bull. 43 (2008) 2509.

19. E. Kendrick, P.R. Slater; Solid State Ionics 179 (2008) 981.

20. P.J. Panteix, I. Julien, P. Abelard, D. Bernache-Assolant; Ceram. Int. 34 (2008) 1579.

21. T. Iwata, K. Fukuda, E. Bechade, O. Masson, I. Julien, E. Champion, P. Thomas; Solid State Ionics 178 (2008) 1523.

22. R. Ali, M. Yashima, Y. Matsushita, H. Yoshioka, K. Okoyama, F. Izumi; Chem. Mater. 20 (2008) 5203.

23. E. Kendrick, D. Headspith, A. Orera, D.C. Apperley, R.I. Smith, M.G. Francesconi, P.R. Slater; J. Mater. Chem. 19 (2009), 749.

24. E. Rodriguez-Reyna, A.F. Fuentes, M. Maczka, J. Lanuza, K. Boulahya, U. Amador; Solid State Sciences 8 (2006)168-177.

25. L. Leon-Reina, E.R. Losilla, M. Martinez-Lara, S. Bruque, A. Llobet, D.V. Sheptyakov, M.A.G. Aranda; J. Mater. Chem. 15 (2005) 2489.

26.P.R. Slater, J.E.H. Sansom, J.R. Tolchard; Chem. Record 4(6) (2004), 373

27. A. Orera, P.R. Slater; Solid State Ionics (2009); doi 10.1016/j.ssi.2008.12.014

28. E. Kendrick, K.S. Knight, P.R. Slater; Mater. Res. Bull. 44 (2009) 1806.

29. J.M. Porras-Vazquez, E.R. Losilla, L. Leon-Reina, D. Marrero-Lopez, M.A.G. Aranda; J. Am. Ceram. Soc. 92 (2009) 1062.

30. C. Bonhomme, S. Beaudet-Savignat, T. Chartier, P-M. Geffroy, A-L. Sauvet ; J. Euro. Ceram. Soc. 29 (2009) 1781.

31. A. Al-Yasari, A. Jones, D.C. Apperley, D. Driscoll, M.S. Islam, P.R. Slater; J. Mater. Chem. 19 (2009) 5003.

32. E. Bechade, O. Masson, T. Iwata, I. Julien, K. Fukuda, P. Thomas, E. Champion; Chem. Mater. 21 (2009) 2508.

33. E. Kendrick, A. Orera, P.R. Slater ; J. Mater. Chem. 19 (2009) 7955.

34. J.D. Gale; J. Chem. Soc., Faraday Trans. 93 (1997) 629.

35. J.D. Gale, A.L. Rohl; Mol. Simul. 29 (2003) 291.

36. C.R.A. Catlow; Computer Modelling in Inorganic Crystallography, Academic Press, San Diego, USA, (1997) 340.

37. M.S. Islam; J. Mater. Chem. 10 (2000) 1027.

38. B. Ammundsen, G.R. Burns, M.S. Islam, H. Kanoh, J. Roziere; J. Phys. Chem. 103 (1999) 5175.

39. S. S. Pramana, T. J. White, M. K. Schreyer, C. Ferraris, P. R. Slater, A. Orera, T. J. Bastow, S. Mangold, S. Doyle, T. Liu, A. Fajar**,** M. Srinivasan, T. Baikie; Dalton Trans., 39 (2009) 8280-8291

Table 1 (from [19]). Conductivity and activation energy values for different compositions

Composition	**Conductivity at 800°C [S/cm]**	**Activation energy [eV]**
$La_8Ba_2(GeO_4)_6O_2$	$2.1x10^{-5}$	1.32
$La_{8.4}Ba_{1.6}(GeO_4)_6O_{2.2}$	$2.2x10^{-3}$	1.08
$La_{8.8}Ba_{1.2}(GeO_4)_6O_{2.4}$	$1.1x10^{-2}$	1.03
$La_{9.2}Ba_{0.8}(GeO_4)_6O_{2.6}$	$2.2x10^{-2}$	1.03
$La_{8.6}Ba_{1.2}(GeO_4)_6O_{2.1}$	$1.1x10^{-2}$	1.03
$La_{8.83}Ba_{0.75}(GeO_4)_6O_2$	$1.1x10^{-2}$	0.99

List of Figures

Figure 1.

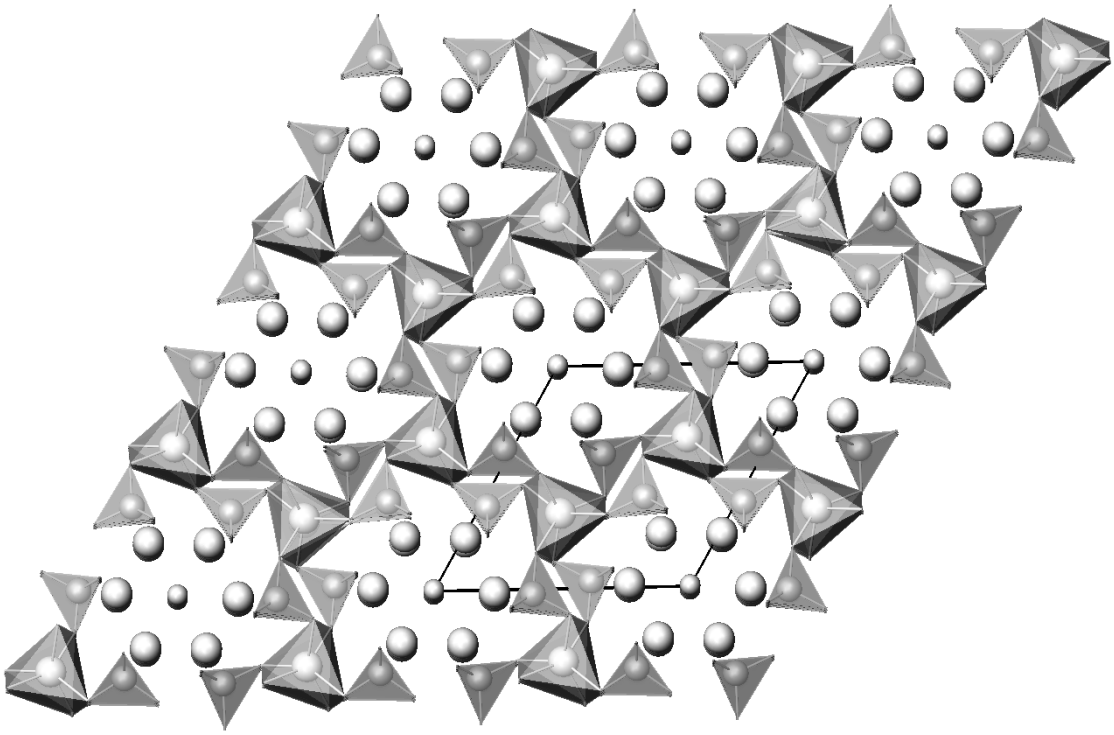

Figure 2.

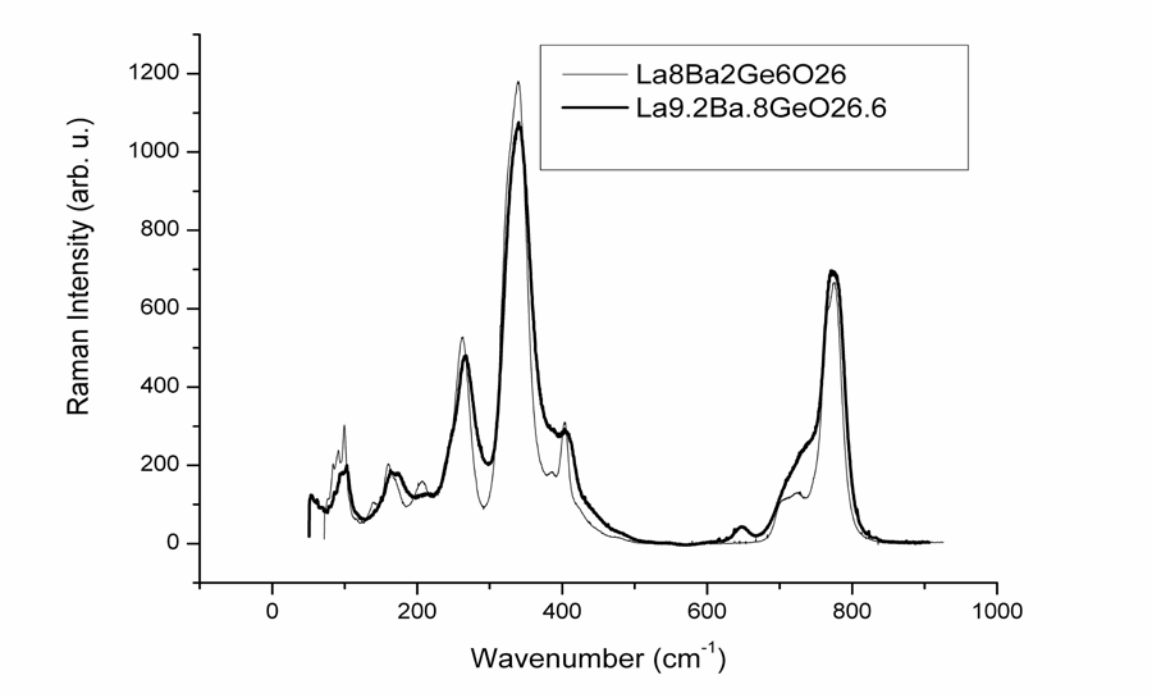
La8Ba2Ge6O26
La9.2Ba.8GeO26.6
Raman Intensity (arb. u.)
Wavenumber (cm-1)
0
200
400
600
800
1000
1200

Figure 3.

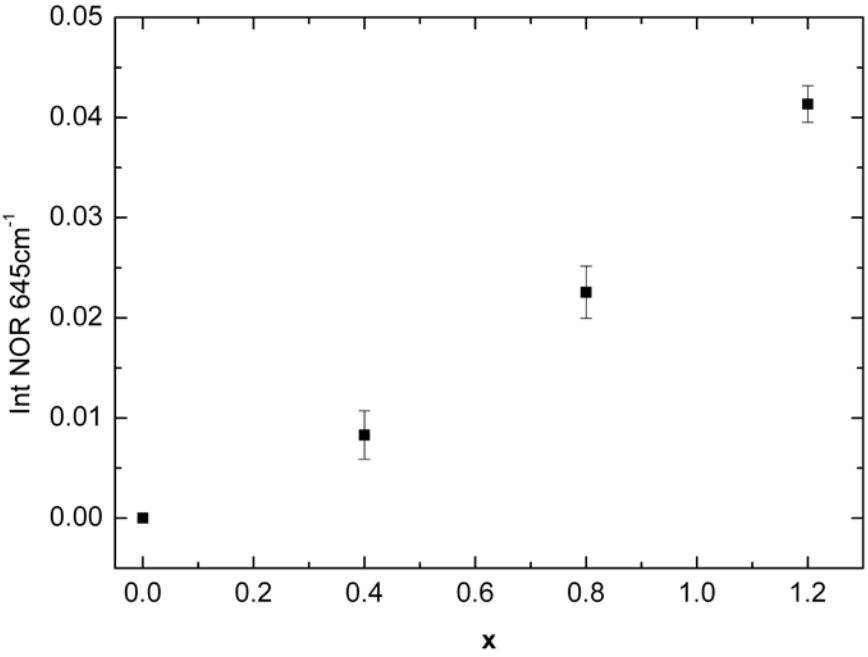

Figure 4.

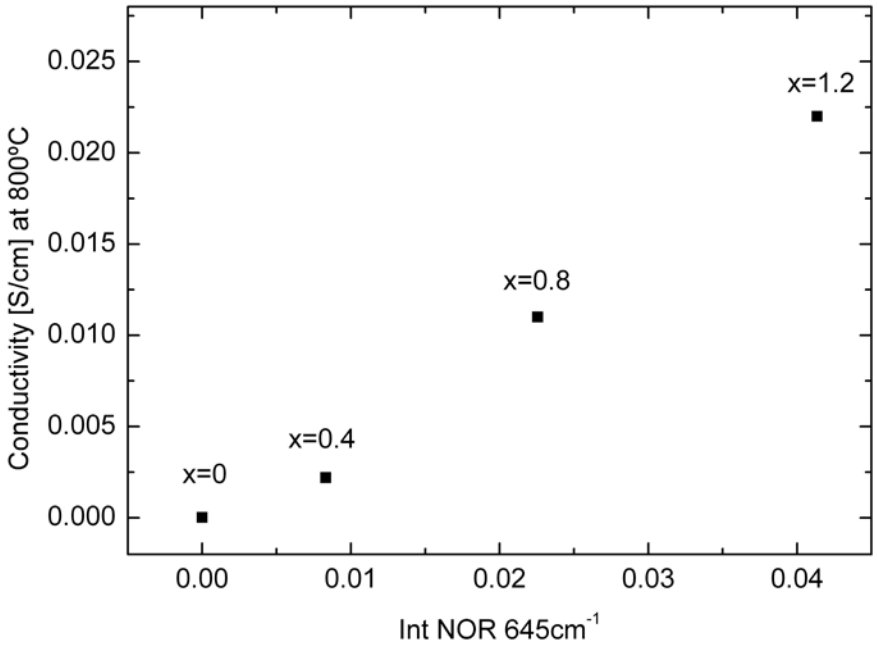
Conductivity [S/cm] at 800ºC
0.025
0.020
0.015
0.010
0.005
0.000
x=1.2
x=0.8
x=0.4
x=0
0.00
0.01
0.02
0.03
0.04
Int NOR 645cm-1

Figure 5.

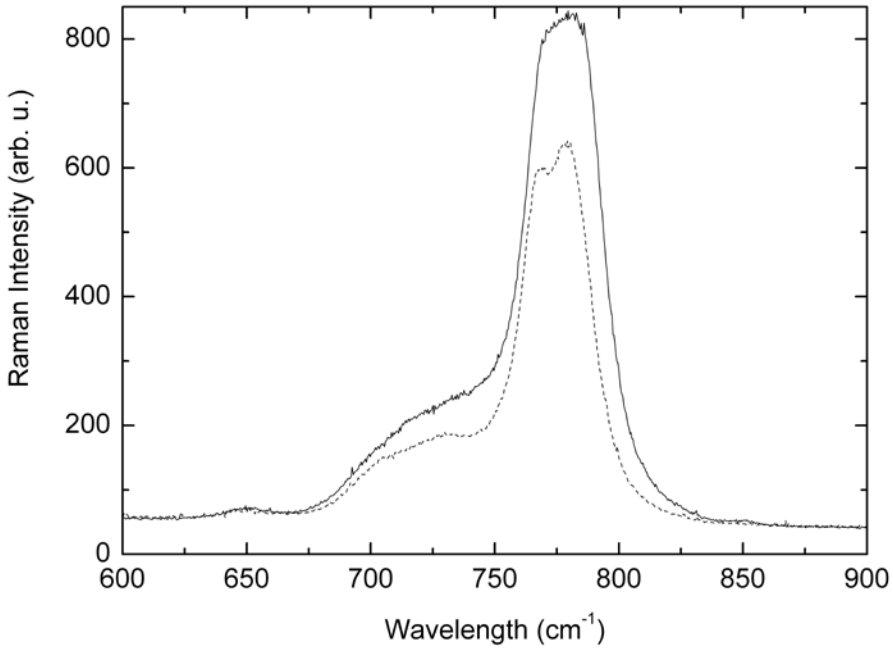
Raman Intensity (arb. u.)
0
200
400
600
800
600
650
700
750
800
850
900
Wavelength (cm-1)

Figure 6.

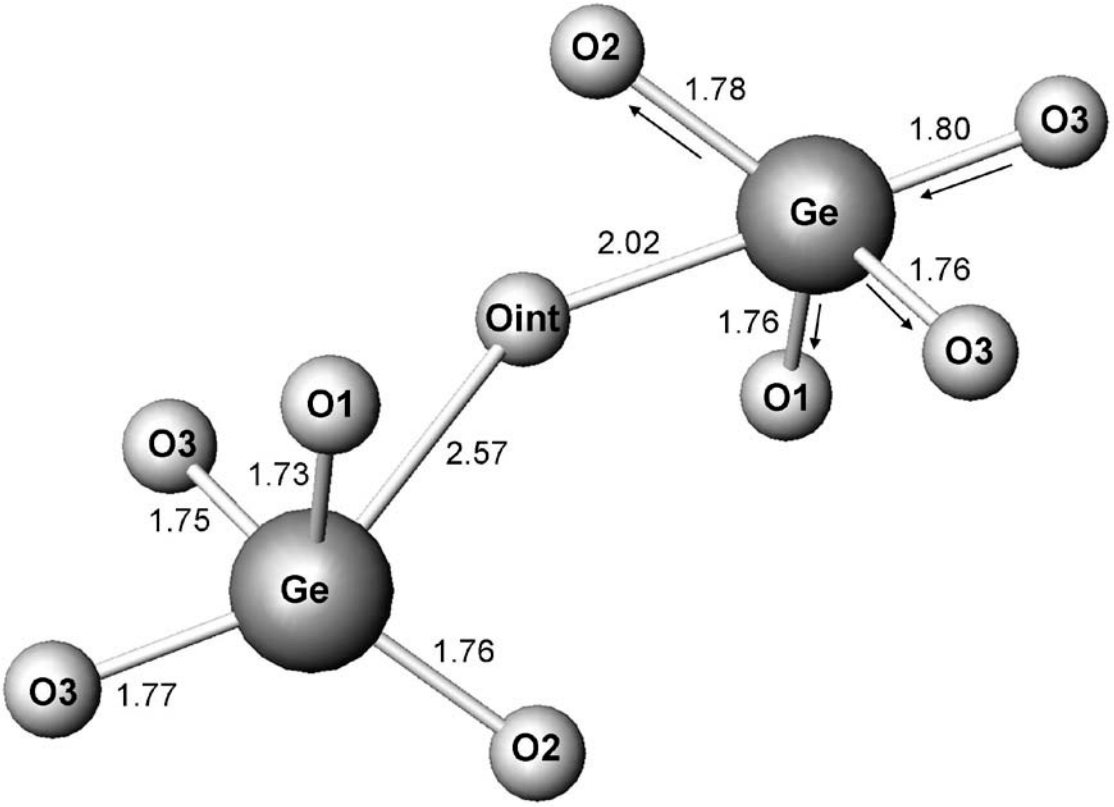
O2
1.78
1.80
O3
Ge
2.02
1.76
Oint
1.76
O3
O1
O1
O3
1.73
2.57
1.75
Ge
1.76
O3
1.77
O2

Figure 7.

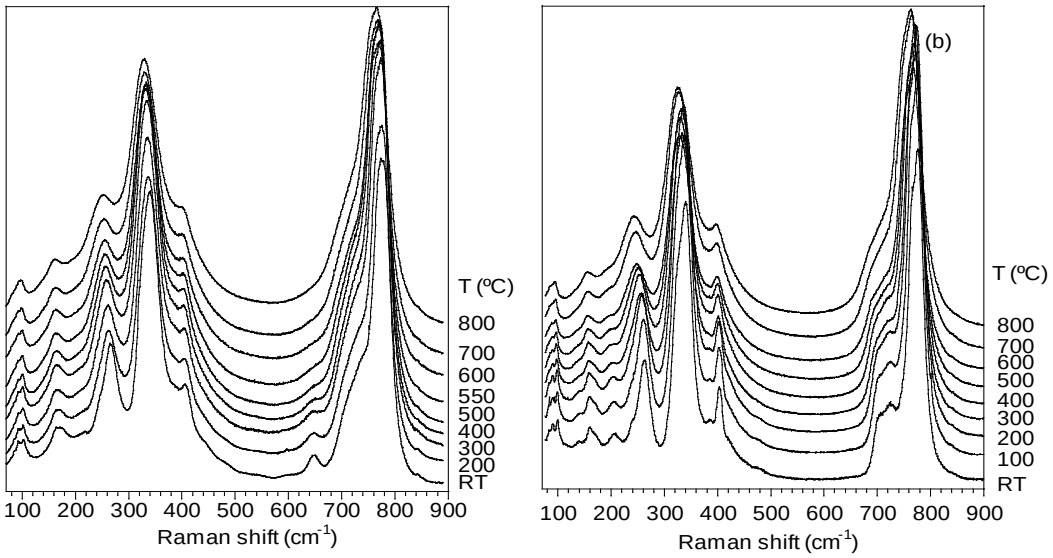
T (ºC)
800
700
600
550
500
400
300
200
RT
100 200 300 400 500 600 700 800 900
Raman shift (cm-1)
(b)
T (ºC)
800
700
600
500
400
300
200
100
RT
100 200 300 400 500 600 700 800 900
Raman shift (cm-1)

Figure 8.